

Quadrupole Effects on Nuclear Magnetic Resonance Gyroscopes

Yue Chang,^{1,2,*} Shunag-Ai Wan,^{1,2} and Jie Qin^{1,2}

¹*Beijing Automation Control Equipment Institute, Beijing 100074, China*

²*Quantum Technology R&D Center of China Aerospace Science and Industry Corporation, Beijing 100074, China*

Nuclear magnetic resonance gyroscopes that detect rotation as a shift in the precession frequency of nuclear spins, have attracted a lot of attentions. Under a feedback-generated drive, the precession frequency is supposed to be dependent only on the angular momentum and an applied magnetic field. However, nuclei with spins larger than $1/2$, experience electric quadrupole interaction with electric field gradients at the cell walls. This quadrupole interaction shifts the precession frequencies of the nuclear spins, which brings inaccuracy to the rotation measurement as the quadrupole interaction constant C_q is difficult to precisely measure. In this work, the effects of quadrupole interaction on nuclear magnetic resonance gyroscopes is theoretically studied. We find that, when the constant C_q is small compared to the characteristic decay rate of the system, as the strength of the feedback-driving field increases, the quadrupole shift monotonically decreases, regardless of the sign of C_q . In large C_q regime, more than one precession frequency exists, and the nuclear spins may precess with a single frequency or multi-frequencies depending on initial conditions. In this regime, with large driving amplitudes, the nuclear spin can restore the single-frequency-precession. These results are obtained by solving an effective master equation of the nuclear spins in a rotating frame, from which both the steady-state solutions and dynamics of the system are shown.

I. INTRODUCTION

Nuclear magnetic resonance gyroscopes (NMRGs) accomplish rotation detection by measuring a shift in the nuclear spins' precession frequency in an applied magnetic field [1–7]. As an inertial navigation system, a NMRG has advantages such as high precision and compact size. Thus, it has attracted much attentions in several decades. A NMRG with basic elements is schematically shown in Fig. 1, where a rotating atomic vapor cell (with its angular momentum along the z direction) contains alkali-metal atoms and noble gas. Usually there is some buffer gas (not shown in Fig. 1) to reduce radiation trapping [8] and wall-collisions of the alkali atoms. A static magnetic field \vec{B}_0 along the z direction is applied in this atomic cell, and a circularly polarized laser is used to optically pump [9–12] the alkali atoms. Then the noble gas are polarized via spin exchange [13–17] with the polarized alkali atoms, and in presence of a feedback-generated AC magnetic field along the x axis, the noble-gas nuclear spins precess with a frequency that depends on the applied magnetic field and rotation of the system. This precession frequency is then measured by the in-situ alkali-metal-vapor atomic magnetometer [14, 18–20], where the alkali atoms's polarization is probed by a linearly polarized laser.

However, the nuclear precession frequency of the noble gas can be shifted by quadrupole interactions [21]. It is given by Wigner-Eckart theorem [22] that all nuclei with spins larger than $1/2$ have quadrupole moments. For instance, to stabilize the magnetic field, dual-isotope NMRGs are used [3, 23], where one of these two isotopes in the commonly used schemes has its nuclear spin

larger than $1/2$. This quadrupole interaction [24–29], resulting from collisions of the noble gas atoms with the cell walls, brings inaccuracy to the rotation measurement since the quadrupole interaction constant is difficult to be precisely measured. A phase delay β (with respect to the precession of the nuclear spins) in the feedback drive can suppress this frequency shift [3]. It is shown that the precession frequency shift is a monotonic function of β , where the frequency shift is zero at a certain value β_0 . However, β_0 is strongly dependent on the system parameters such as the longitudinal and transverse relaxation rates of the nuclear spins, the sign and strength of the quadrupole interaction constant C_Q , the amplitude of the feedback drive Ω_d , and so on. Thus, to have a reduced frequency shift by tuning β , one needs knowledge of other parameters of the system, especially when the system parameters fluctuate, one needs to know the time dependence of these parameters. It makes this method less practical.

In literature, there are many other researches on the frequency shift [24–27] and nuclear spin relaxation [24, 26, 28] induced by the electric quadrupole interaction, but few are on feedback-driven systems [3]. Therefore, in this paper, we theoretically study the effect of the quadrupole interaction on feedback-driven NMRGs. By solving an effective master equation of the nuclear spins, we find that the absolute value of the quadrupole shift monotonically decreases as the feedback-driving amplitude Ω_d increases, despite other parameters of the system. This can be understood intuitively: the quadrupole interaction brings linearity in the nuclear spin's energy-level spacings, which will shift the resonant frequency in the long-term limit. But increasing the driving amplitude will reduce the relative nonlinearity by reducing the ratio between the difference of the energy-level spacing and the corresponding energy-level spacing. As a result, the frequency shift is reduced. Apart from the frequency

* yuechang7@gmail.com

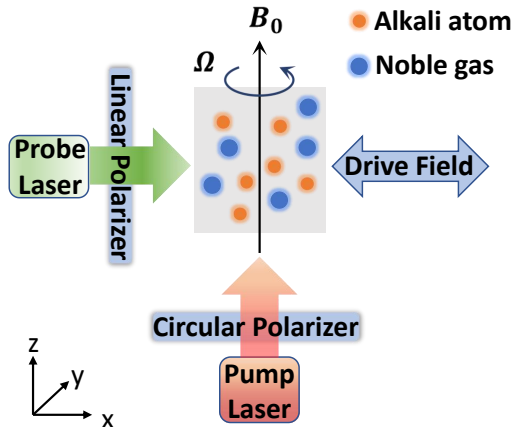


FIG. 1. Schematic of a NMRG, where alkali atoms (orange circles) and noble gas (blue circles) are confined in an atomic cell (usually there is also buffer gas that is not shown in the figure) which is subjected to a rotation and an applied static magnetic field \vec{B}_0 along the z direction. The alkali atoms are optically pumped by a circularly polarized laser, resulting in polarization of the electron spins. This electronic polarization is transferred to nuclear spins of the noble gas by spin-exchange collisions. In presence of a feedback-driven AC magnetic field in the x direction, the polarized nuclear spins precess with a frequency that depending on the rotation and the applied field \vec{B}_0 . This precession frequency is acquired by measuring the optical rotation using a linearly-polarized laser with the in-situ alkali-metal-vapor atomic magnetometer.

shift, we show that the the quadrupole interaction reduces the nuclear precession magnitude because of the destructive interference of oscillations between adjacent states of the nuclear spins. In principle, this reduction can be compensated by increasing the density of the noble gas while keeping a relatively high sensitivity of the in-situ atomic magnetometer.

For large quadrupole interaction, more than one precession frequency exists. In this case, the nuclear spin precesses with one or multi-frequencies depending on its initial condition. We study the dynamics of the nuclear spins for different initial states. We show that increasing Ω_d can stimulate more oscillations with different frequencies. However, when the driving amplitude Ω_d is sufficiently large, the nuclear spin restores the single-frequency precession. The mechanism is the same as in the small- Ω_d regime: large driving amplitude can reduce the nonlinearity coming from the quadrupole interaction.

The rest of the paper is organized as follows. In Sec. II, we give the effective master equation for the noble gas' nuclear spins, which is obtained by neglecting correlations between the alkali atoms and noble gas atoms and eliminating the alkali atoms' degrees of freedom. In Sec. III, we write the master equation in a rotating frame with respect to the feedback driving frequency that needs

to be determined. The long-term behaviors of the precession frequency are shown from symmetry analysis of this master equation with a time-independent Liouvillian. Then in In Sec. IV, we numerically solve this master equation and show the steady-state behaviors as functions of the driving amplitude Ω_d . The absolute value of the frequency shift decreases monotonically as Ω_d increases. For comparison, we also show the quadrupole shift as a function of the phase shift β . As the quadrupole interaction constant C_Q increases, the system may exhibit more than one precession frequencies. This situation is studied in Sec. V, where we show dynamics of the nuclear spins for various initial conditions and driving amplitude Ω_d . Finally, in Sec. VI, we summarize our results.

II. EFFECTIVE MASTER EQUATION FOR NUCLEAR SPINS WITH NONZERO QUADRUPOLE MOMENTS

In this section, we will give the effective master equation of the noble-gas nuclei. The master equation constitutes a unitary-evolution part which is describe by a system Hamiltonian H and dissipations $\mathcal{L}_D[\rho]$ [30, 31]:

$$\partial_t \rho = -i[H, \rho] + \mathcal{L}_D[\rho], \quad (1)$$

where ρ is the density matrix of the noble-gas's nuclear spin. The Hamiltonian contains three terms

$$H = \omega_0 K_z + C_Q K_z^2 + \Omega_d K_x \sin(\phi - \beta), \quad (2)$$

where K_j with $j = x, y, z$, is the nuclear spin operator of the noble gas. The first term in H is the interaction of the nuclear spins to constant applied fields: an applied magnetic field $B_0 \hat{e}_z$ and rotation of the gyroscope apparatus along the z direction with frequency Ω (see Fig. 1). Thus, the "ideal" precession frequency ω_0 of the noble gas' nuclear spin in the laboratory frame is

$$\omega_0 = \gamma B_0 \mp \Omega, \quad (3)$$

where γ is the gyromagnetic ratio and the sign " \mp " depicts that the angular momentum is in the $\pm z$ direction. The second term in H is the quadrupole interaction to collision-induced electric gradients at the cell walls. It is this quadrupole interaction which results in deviation of the nuclear spin's actual precession frequency from the ideal one ω_0 . Here, we have assumed the atomic cell is a z -axial cylinder, or a z -axial right regular prism excluding a cube. Averaging over the sticking time and the entire inner surface of the vapor cell, one can acquire the quadrupole interaction Hamiltonian simply as $C_Q K_z^2$ [25], where a constant that depends on the nuclear spin K has been neglected. To drive the nuclear spins to precess at its resonant frequency ω_0 , a feedback-generated ac magnetic field in the x -direction is applied. The amplitude Ω_d of this oscillating field is a constant,

but the phase ϕ is feedback generated via the phase of $\langle K_+ \rangle \equiv \langle K_x + iK_y \rangle$, i.e., ϕ is defined through

$$\langle K_+ \rangle \equiv K_\perp e^{-i\phi}, \quad (4)$$

where K_\perp is the absolute value of $\langle K_+ \rangle$. Here, a constant phase delay β is employed, which can suppress the quadrupole shift [3]. For small driving amplitude Ω_d so that the actual precession frequency is much larger than Ω_d , we can utilize the rotating-wave approximation to H as

$$H = \omega_0 K_z + C_Q K_z^2 + \frac{\Omega_d}{4i} \left(K_+ e^{i(\phi-\beta)} - K_- e^{-i(\phi-\beta)} \right), \quad (5)$$

where we have neglected the fast-oscillating terms that oscillate with twice of the precession frequency.

To acquire enhanced precession signals of the nuclear spins from collective effects, nuclear spins are polarized through spin-exchange interaction (Fermi-contact hyperfine interaction) with alkali atoms [13, 14, 16, 17]:

$$H_{se} = \alpha(R) \vec{K} \cdot \vec{S}, \quad (6)$$

where \vec{S} is the electron spin operator of the alkali atom, $\alpha(R)$ is the coupling coefficient depending on the inter-nuclear separation R between the alkali atom and noble gas atom. It is known that this Fermi-contact hyperfine interaction transfers electron spins to nuclear spins in two ways [13, 14]: through binary collisions between a pair of an alkali atom and a noble gas atom, and through three-body-collision formed weakly-bound van der Waals molecules in presence of the buffer gas. Tracing out the alkali atom's degrees of freedom by neglecting correlations between alkali atoms and noble gas nuclei, we have spin-exchange induced dissipation as [32]

$$\begin{aligned} \mathcal{L}_{se}[\rho] &= \Gamma_S \left[\vec{K} \cdot \rho \vec{K} - \frac{1}{2} \{ \rho, K^2 \} \right] \\ &+ 2\Gamma_f \langle F_z^2 \rangle [2K_z \rho K_z - \{ \rho, K_z^2 \}] \\ &+ \Gamma_f \langle F^2 - F_z^2 \rangle [K_+ \rho K_- + K_- \rho K_+ - \{ \rho, K^2 - K_z^2 \}] \\ &+ \Gamma_p [K_+ \rho K_- - K_- \rho K_+ + \{ \rho, K_z \}], \end{aligned} \quad (7)$$

where $\Gamma_S = \Gamma_{bin} + \Gamma_s$ is the total S-damping rate, with the binary collision rate Γ_{bin} , Γ_s/Γ_f is the exchange rate originating from the short/long-lived van der Waals molecules, and $\Gamma_p = \Gamma_S \langle S_z \rangle + \Gamma_f \langle F_z \rangle$ is the polarization rate. Here, $F = I + S$, where I is the nuclear spin of the alkali atom. Consequently, taking into account the nuclear spin's longitudinal and transverse relaxation due to other mechanisms, we have the dissipation term in the master equation (1) as

$$\begin{aligned} \mathcal{L}_D[\rho] &= \Gamma_1 \left[\vec{K} \cdot \rho \vec{K} - \frac{1}{2} \{ \rho, K^2 \} \right] + \Gamma_2 [2K_z \rho K_z - \{ \rho, K_z^2 \}] \\ &+ \Gamma_p [K_+ \rho K_- - K_- \rho K_+ + \{ \rho, K_z \}], \end{aligned} \quad (8)$$

where $\Gamma_1 = \Gamma'_1 + \Gamma_S + 2\Gamma_f \langle F^2 - F_z^2 \rangle$ and $\Gamma_2 = \Gamma'_2 + 2\Gamma_f \langle 2F_z^2 - F^2 \rangle$, with $\Gamma'_{1,2}$ the relaxation rate from wall collisions, magnetic field gradients, and other possible mechanisms rather than the spin-exchange interaction.

We note that in the master equation (1), the effective magnetic field from the electron magnetization has been ignored since it is very small compared to ω_0 . And because of the much slower dynamics of the nuclear spins compared to the typical time scale of the the alkali atoms' z -directional polarization, $\Gamma_{1,2,p}$ in Eq. (8) can be treated as constants. In spite of these simplification, Eq. (1) is still a nonlinear equation whose exact solution can only be obtained numerically. Before we do the numerics, in Sec. III, we will show some properties of the actual nuclear precession frequency in the long-term limit.

III. MASTER EQUATION IN A ROTATING FRAME

In this section, we will write Eq. (1) in a rotating frame with a time-independent Liouvillian. For this purpose, we assume the long-time behavior of ϕ can be written as $\phi = -(\omega_0 - \omega)t + \theta_0$, where ω is the deviation of the actual precession frequency from the ideal one, and θ_0 is a constant phase. This assumption is valid when the quadrupole interaction constant C_Q is small compared to the characteristic decay rate of the system. Note that the system has $U(1)$ symmetry, i.e., the master equation (1) is invariant under the transformation $\rho \rightarrow e^{iK_z \theta} \rho e^{-iK_z \theta}$, and $K_+ \rightarrow K_+ e^{i\theta}$. As a result, the steady state has a phase uncertainty, which is determined by initial conditions. Since we only concern the precession frequency, for simplicity, θ_0 is set to be zero here. Then, in a rotating frame with $\tilde{\rho} = e^{iK_z(\omega_0 - \omega)t} \rho e^{-iK_z(\omega_0 - \omega)t}$, the master equation can be rewritten as

$$\partial_t \tilde{\rho} = -i [\tilde{H}, \tilde{\rho}] + \mathcal{L}_D[\tilde{\rho}]. \quad (9)$$

where the Hamiltonian (with rotating-wave approximation) in the rotating frame is

$$\tilde{H} = \omega K_z + C_Q K_z^2 + \frac{\Omega_d}{4i} (K_+ e^{-i\beta} - K_- e^{i\beta}). \quad (10)$$

This master equation with the time-independent Liouvillian has a steady-state solution $\tilde{\rho}_s$ which is a function of ω that needs to be determined. Back to the original frame, the average value of K_+ in the long-term limit is

$$\langle K_+ \rangle = \text{Tr} (K_+ \tilde{\rho}_s) e^{i(\omega_0 - \omega)t}. \quad (11)$$

As a result, ω_s , the solution of ω is determined via the condition

$$\text{angle} [\text{Tr} (K_+ \tilde{\rho}_s)] = 0, \quad (12)$$

i.e.,

$$k_y(\omega_s, \Omega_d, C_Q, \beta) \equiv \text{Tr} (K_y \tilde{\rho}_s) = 0 \quad (13)$$

and

$$k_x(\omega_s, \Omega_d, C_Q, \beta) \equiv \text{Tr}(K_x \tilde{\rho}_s) > 0. \quad (14)$$

Performing the time-reversal transformation \mathcal{T} that gives $\mathcal{T}K_y\mathcal{T}^{-1} = -K_y$ and $\mathcal{T}i\mathcal{T}^{-1} = -i$, one can acquire that the dissipation \mathcal{L}_D remains unchanged, but the Hamiltonian \tilde{H} becomes

$$\mathcal{T}\tilde{H}\mathcal{T}^{-1} = \omega K_z + C_Q K_z^2 - \frac{\Omega_d}{4i} (K_+ e^{i\beta} - K_- e^{-i\beta}).$$

Taking into account of the sign change of i in the master equation, we have

$$k_x(\omega, \Omega_d, C_Q, \beta) = k_x(-\omega, \Omega_d, -C_Q, -\beta) \quad (15)$$

and

$$k_y(\omega, \Omega_d, C_Q, \beta) = -k_y(-\omega, \Omega_d, -C_Q, -\beta). \quad (16)$$

Eq. (16) shows that in absence of the quadrupole interaction, $k_y(\omega = 0) = 0$ when the phase delay $\beta = 0$. In this case, $\omega = 0$ may be a solution, depending on whether $k_x(\omega, \Omega_d, C_Q, \beta) > 0$. To further study it, we perform a unitary transformation

$$U = \exp(i\pi K_z), \quad (17)$$

which is actually a π -rotation along the z -axis, to the master equation 9. This transforms $K_x \rightarrow -K_x$ and $K_y \rightarrow -K_y$. So we obtain

$$k_{x,y}(\omega, \Omega_d, C_Q, \beta) = -k_{x,y}(\omega, -\Omega_d, C_Q, \beta). \quad (18)$$

Namely, when the sign of Ω_d is changed, the sign of $k_{x,y}$ is also changed. Considering that the solution ω_s requires positive $k_x(\omega_s, \Omega_d, C_Q, \beta)$, we can conclude that in absence of the quadrupole interaction, either positive or negative Ω_d enables the nuclear spin to precess with the ideal frequency ω_0 .

In presence of the quadrupole interaction, the frequency deviation ω_s is nonzero. One way to suppress it is to employ the phase shift β , as shown in Ref. [3]. However, to determine β , one needs the knowledge of C_Q . In fact, it can also be seen from Eq. (16) that when the sign of C_Q changes, the sign of β should also be changed to insure $k_y(\omega_s = 0) = 0$. Since C_Q is difficult to measure accurately, we propose another solution to reduce the quadrupole shift: in next section, we will show that increasing the driving strength $|\Omega_d|$ will monotonically reduce the quadrupole shift $|\omega_s|$, despite other system parameters.

IV. REDUCTION OF THE QUADRUPOLE SHIFT

In this section, we will numerically solve the master equation 9 and acquire the precession-frequency shift

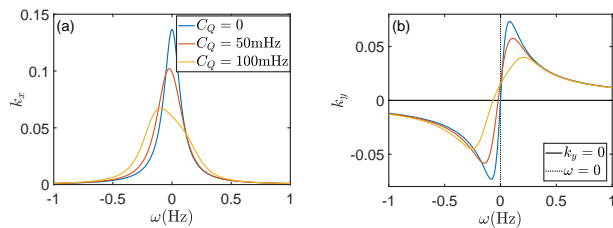


FIG. 2. Average values (a) k_x and (b) k_y as functions of ω with different quadrupole interaction strength C_Q for the spin-3/2 case. Other parameters are: $\Gamma_1 = \Gamma_2 = 1/20$ Hz, $\Omega_d = 1/20$ Hz, $\beta = 0$. With positive Ω_d , k_x is always positive, as shown in (a). Thus, negative Ω_d will not give a nontrivial solution of ω since the solution requires that $k_x > 0$, and Eq. (18) gives that $k_x < 0$ for negative Ω_d . In (b), the intersection of k_y and the $k_y = 0$ line (solid black line) gives the solution ω_s , and the dotted black line shows the $\omega = 0$ case. It is shown that with positive C_Q , the frequency deviation is negative, while Eq. (16) gives that the frequency deviation is positive for negative C_Q . When C_Q increases, the absolute value of the deviation also increases.

ω_s . We first need to determine whether positive or negative Ω_d gives zero frequency deviation in absence of the phase delay β and quadrupole interaction. Without loss of generality, we consider a nucleus with spin 3/2, which is the nuclear spin of ^{131}Xe that is commonly used in dual-isotope NMRs. With other parameters $\Gamma_1 = \Gamma_2 = 1/20$ Hz, $\Omega_d = 1/20$ Hz, $\beta = 0$, we plot $k_{x,y}$ as functions of ω for different quadrupole interaction constants C_Q in Fig. 2. Fig. 2(a) shows that k_x is positive with positive Ω_d . Thus, from the requirement that $k_x(\omega_s, \Omega_d, C_Q, \beta)$ must be positive and Eq. (18), we conclude that negative Ω_d does not give nontrivial solutions of ω . Thus, in the rest of the paper, we will consider positive Ω_d only. With positive k_x , ω_s is determined by $k_y(\omega) = 0$, which is the intersection of k_y with the solid black line in Fig. 2(b). It is shown that when $C_Q > 0$, the actual precession frequency deviate from the ideal one ω_0 . This deviation becomes larger when C_Q increases.

The dependence of the deviation ω_s and the average value k_x on the quadrupole interaction constant C_Q is shown in Figs. 3(a) and (b) with different driving amplitudes Ω_d , while other parameters are the same as in Fig. 2. When C_Q increases, the actual precession frequency deviates more from ω_0 . This brings inaccuracy to the measurement on the precession frequency, because the exact quadrupole interaction strength C_Q is difficult to measure. Meanwhile, as shown in Fig. 3(b), k_x , which is K_\perp , the precession amplitude in the original frame, decreases. Noting that in the basis $|m\rangle$ ($m = -K, \dots, K$), which is the eigenstate of K_z : $K_z|m\rangle = m|m\rangle$, K_x is

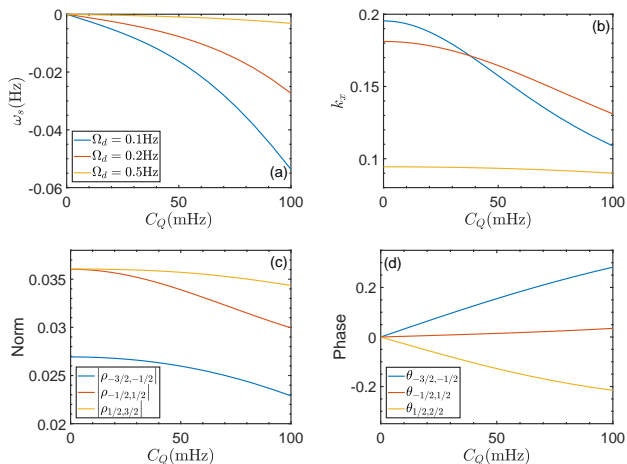


FIG. 3. (a) Precession frequency deviation ω_s and (b) average value k_x as functions of the quadrupole interaction constant C_Q at different amplitudes Ω_d of the drive. The legend in (b) is the same as (a). It shows that, when C_Q increases, the norm of the frequency deviation ω_s increase, while k_x , the precession amplitude decrease. The later is resulted from the decrease of the norm $|\rho_{m,m+1}|$ and the difference of the phase $\theta_{m,m+1}$ of $\rho_{m,m+1}$, which are shown in (c) and (d) with $\Omega_d = 0.2\text{Hz}$.

written as

$$K_x = \frac{\sqrt{3}}{2} \left| \frac{3}{2} \right\rangle \left\langle \frac{1}{2} \right| + \left| \frac{1}{2} \right\rangle \left\langle -\frac{1}{2} \right| + \frac{\sqrt{3}}{2} \left| -\frac{1}{2} \right\rangle \left\langle -\frac{3}{2} \right| + \text{H.c.}, \quad (19)$$

we plot the norm $|\rho_{m,m+1}|$ and phase $\theta_{m,m+1}$ of density matrix elements $\rho_{m,m+1} \equiv \langle m | \tilde{\rho}_s | m+1 \rangle$ where $m = -3/2, -1/2$, and $1/2$, in Figs. 3(c) and (d) with $\Omega_d = 0.2\text{Hz}$ while other parameters the same as in Figs. 3(a) and (b). Figs. 3(c) and (d) show that the decrement of k_x results from two sources: the norm $|\rho_{m,m+1}|$ decreases and the phase $\theta_{m,m+1}$ is nonzero. Both of these comes from the destructive interference between oscillations (in the original frame) between states $|m\rangle$ and $|m+1\rangle$: because of the quadrupole interaction, the inherent energies of states $|m\rangle$ and $|m+1\rangle$ are different (the eigenvalues of \tilde{H} with $\Omega_d = 0$). Thus, in presence of the dissipation and feedback drive, in the steady state, all these oscillation frequencies become $\omega_0 - \omega_s$, but with different phases of $\rho_{m,m+1}$, which leads to destructive interference in the amplitude K_\perp .

The decrement of the precession amplitude can be compensated by increasing the density of the noble gas, but the deviation of the precession frequency remains problematic. By increasing the driving amplitude Ω_d , we find that the deviation of the precession frequency decreases, as shown in Fig. 4(a), with other parameters the same as in Fig. 3. Since Eq. (16) gives that the solution ω_s is inverted when the the quadrupole interac-

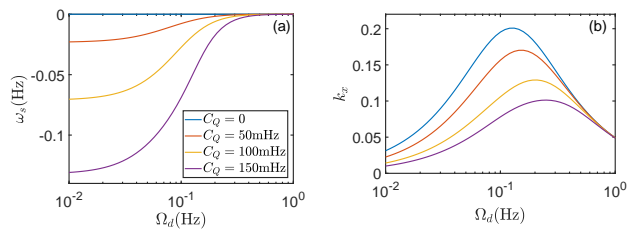


FIG. 4. (a) ω_s as a function of the driving amplitude Ω_d , for different quadrupole interaction constant C_Q . It shows that $|\omega_s|$ decreases monotonically when Ω_d increases. At large Ω_d , the system behaves like a system without quadrupole interaction. This can be seen from (b), where for different values of C_Q , k_x converges to a value in the $C_Q = 0$ case.

tion constant C_Q is inverted, we conclude that the absolute value $|\omega_s|$ monotonically decreases by increasing Ω_d . Physically, this can be explained intuitively: with larger Ω_d , the nonlinear effect of the quadrupole interaction is relatively smaller. Namely, the eigenvalues of the Hamiltonian \tilde{H} ($\beta = 0$) is relatively more equally spaced. In this case, the system is closer to a system without quadrupole interaction. This can be shown in Fig. 4(b), where at large Ω_d limit, for different values of C_Q , k_x with $C_Q > 0$ coincides with the curve with $C_Q = 0$.

Another way to reduce the quadrupole shift is by tuning the phase delay β [3]. The change of ω_s as a function of β is shown in Fig. 5a, where $\Omega_d = 0.1\text{Hz}$ and other parameters the same as in Fig. 4. Here, the intersection with the black line gives a value β_0 that makes $\omega_s = 0$. Around β_0 , $|\omega_s|$ is smaller than in the $\beta = 0$ case. However, β_0 is strongly depending on the system parameters. For instance, when C_Q becomes $-C_Q$, β_0 changes to $-\beta_0$ (Eq. (16)). As a result, to reduce $|\omega_s|$ by tuning the phase delay β , one would need the knowledge C_Q , which makes it less practical than simply increasing the driving amplitude Ω_d . Moreover, tuning β does not help to increase the precession amplitude, as show in Fig. 5b. Therefore, in the following, we only focus on the case with $\beta = 0$.

So far, we have studied the precession frequency in a relatively small quadrupole interaction regime, where only one precession frequency exists. In the next section, we will show that when C_Q becomes large, more precession frequencies appear.

V. LARGE C_Q REGIME: MULTI-PRECESSION-FREQUENCIES

For small quadrupole interaction constant C_Q , in the long-term limit, only one precession frequency exists, and increasing the driving amplitude can monotonically decrease the frequency deviation. However, this is not the case for large C_Q , where the quadrupole splitting ($2C_Q$ for spin-3/2) is not much smaller than the characteristic

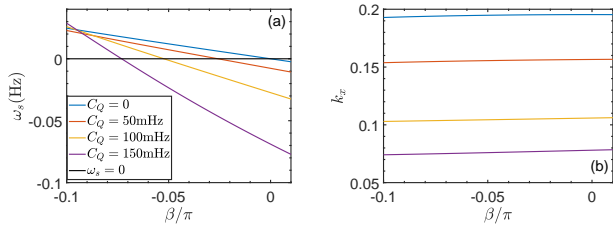


FIG. 5. (a) Precession frequency deviation ω_s and (b) precession amplitude k_x as functions of the phase delay β for different values of C_Q . The black line in (a) has $\omega_s = 0$, and its intersection with the curves gives a value β_0 that makes $\omega_s = 0$. This value β_0 varies with different C_Q . Meanwhile, (b) shows that as the phase delay β changes, the precession amplitude k_x almost remains unchanged.

decay rate of the system that is determined by the relaxation rates $\Gamma_1, \Gamma_2, \Gamma_p$, and the driving amplitude Ω_d . In this regime, more than one precession frequency appears and the long-term behavior of the system depends on initial conditions of the system.

To separate the fast oscillation with frequency ω_0 , we work in a rotating frame with respect to $\omega_0 K_z$, where the dynamics of the density matrix $\tilde{\rho}'$ is governed by Eq. 9 with $\omega = 0$. In this frame, the average value $k'_+ \equiv \text{Tr}(K_+ \tilde{\rho}')$ is connected to $\langle K_+ \rangle$ in the original frame as

$$\langle K_+ \rangle = k'_+ e^{i\omega_0 t}, \quad (20)$$

and $|k'_+| = K_\perp$. To show how the long-term behavior depends on initial conditions, we plot $\text{Re}[k'_+(t)]$ and K_\perp for two different initial states $\tilde{\rho}'_0$: (a) $\tilde{\rho}'_0 = |3/2\rangle\langle 3/2|$ and (b) $\tilde{\rho}'_0 = I$ in Figs. 6(a) and (b), with $\Omega_d = 0.1\text{Hz}$. In case (a), $\text{Re}[k'_+(t)]$ oscillates with a single frequency and K_\perp is a constant in large- t limit. However, in Figs. 6(b), $\text{Re}[k'_+(t)]$ shows multi-frequencies and its amplitude K_\perp also has oscillations. The Fourier transform of $\mathcal{F}[k'_+]$ gives the precession frequencies, as shown in the peaks in Figs. 6(c) and (d) corresponding to cases (a) and (b), respectively. It is shown that besides a frequency $\nu_0 = 0.91\text{Hz}$ that is the same as in case (a), k'_+ has two more frequencies $\nu_1 = 0.056\text{Hz}$ and $\nu_{-1} = -0.80\text{Hz}$ in case (b). The weights of oscillations with these three frequencies are different, but the differences between the adjacent frequencies are the same (considering the numerical error): $\nu_1 - \nu_0 = \nu_0 - \nu_{-1}$. The reason is because in the Hamiltonian H without drive, the quadrupole interaction $C_Q K_z^2$ causes two more frequencies in oscillations between states $|3/2\rangle$ and $|1/2\rangle$ and states $|-1/2\rangle$ and $|-3/2\rangle$, and the spacing between these two frequencies and the ideal precession frequency ω_0 are equal. Therefore, under the feedback drive and relaxation, $k'_+(t)$ oscillates with equally spaced frequencies.

When the driving amplitude Ω_d increases to 0.5Hz , more oscillations are stimulated, as shown in Fig. 7, where the precession amplitude K_\perp and the nuclear spin's polarization in the x direction $\text{Re}[k'_+(t)]$ are plotted

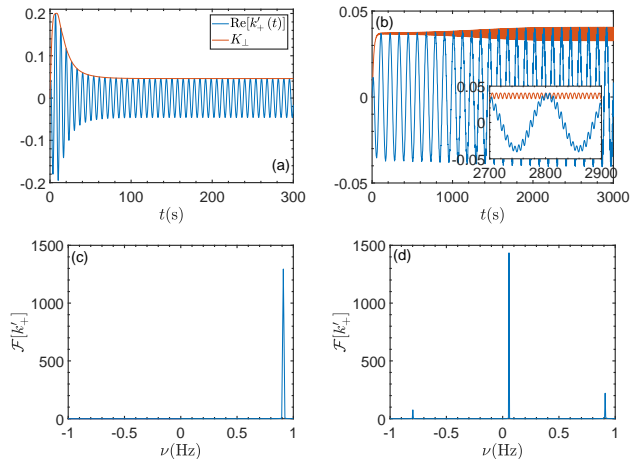


FIG. 6. Nuclear spin polarization along the x direction $\text{Re}[k'_+(t)]$ (in the rotating frame with respect to $\omega_0 K_z$) for different initial states (a) $\tilde{\rho}'_0 = |3/2\rangle\langle 3/2|$ and (b) $\tilde{\rho}'_0 = I$. The Fourier transform of $k'_+(t)$ in the long-term limit from the time domain to frequency domain is shown in (c) and (d), with the corresponding initial condition the same as (a) and (b), respectively. Both the behaviors in time and frequency domains show that the nuclear spins may precess with a single frequency or multi-frequencies, depending on the initial states. One of the frequencies in the latter case is the same as the single frequency in (c), and these multi-frequencies are equally spaced, as shown in (d).

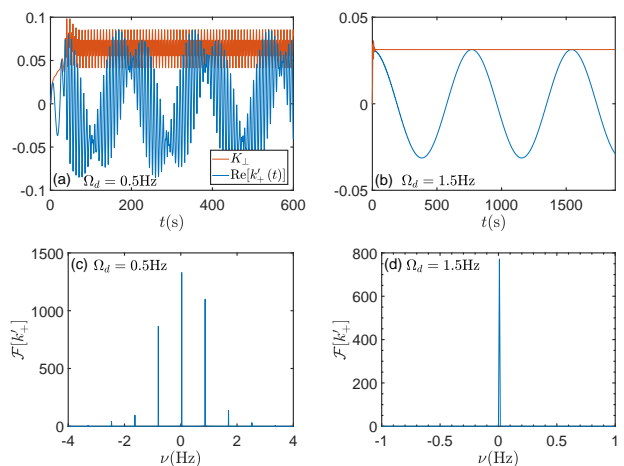


FIG. 7. Same as Fig. 6 for $\tilde{\rho}'_0 = I$, but with different driving amplitudes $\Omega_d = 0.5\text{Hz}$ for (a) and (c), $\Omega_d = 1.5\text{Hz}$ for (b) and (d). Figures (a) and (c) show that increasing Ω_d will increase the number of the precession frequencies. These frequencies are equally spaced. However, the further increment of Ω_d can drive the nuclear spin to precess with a single frequency, as shown in (b) and (d).

in (a), while the Fourier transform $\mathcal{F}[k'_+]$ is plotted in (c). Here, the initial state $\tilde{\rho}'_0 = I$. Similar to the case in Fig. 6(d), the nine oscillations have different weights while the frequencies are equally spaced. As Ω_d is further increased, the system comes back to the small quadrupole interaction case: the nuclear spin precesses with a single frequency, as shown in Fig. 7(b) and (d), with $\Omega_d = 1.5\text{Hz}$. Meanwhile, the frequency deviation (0.008Hz) is smaller than the smallest frequency deviation in cases with smaller Ω_d (0.056Hz for $\Omega_d = 0.1\text{Hz}$ and 0.034Hz for $\Omega_d = 0.5\text{Hz}$). The reason is the same as explained in Sec. V: the nonlinearity resulting from the quadrupole interaction is reduced by very large Ω_d .

VI. CONCLUSION

We have theoretically studied the effects of quadrupole interactions on feedback-generated-driven NMRGs whose nuclear spins are larger than $1/2$. This quadrupole interaction that is resulting from collisions of the noble gas atoms with the cell walls, causes a single shift in the

nuclear spin's precession frequency when the quadrupole interaction constant C_Q is small compared to the characteristic decay rate of the system. Solving the effective master equation of the nuclear spins by neglecting its correlations with the electron spins, we show that the quadrupole shift can be monotonically decreased by increasing the amplitude of the feedback drive.

In large C_Q regime, the nuclear spin may precess with a single frequency or multi-frequencies depending on its initial state, since the master equation is nonlinear. We have studied the dynamics of the system in the long-term limit. It is shown that when the driving amplitude is larger enough, the nuclear spin restores the single-frequency precession.

ACKNOWLEDGMENTS

This work was supported by the National Key R&D Program of China Grant No.2017YFB0503102 and the National Natural Science Foundation of China Grant No.61627806.

-
- [1] J. Simpson, J. Fraser, and I. Greenwood, *IEEE Transactions on Aerospace* **1**, 1107 (1963).
 - [2] D. Bayley, I. Greenwood, and J. Simpson, "Optically pumped nuclear magnetic resonance gyroscope," (1973), uS Patent 3,778,700.
 - [3] T. G. Walker and M. S. Larsen, in *Advances in atomic, molecular, and optical physics*, Vol. 65 (Elsevier, 2016) pp. 373–401.
 - [4] E. A. Donley, in *SENSORS, 2010 IEEE* (IEEE, 2010) pp. 17–22.
 - [5] T. G. Walker, A. Korver, D. Thrasher, and M. Bulatowicz, in *2015 IEEE International Symposium on Inertial Sensors and Systems (ISISS) Proceedings* (IEEE, 2015) pp. 1–4.
 - [6] T. W. Kornack, R. K. Ghosh, and M. V. Romalis, *Phys. Rev. Lett.* **95**, 230801 (2005).
 - [7] E. N. Popov, K. A. Barantsev, and A. N. Litvinov, *Quantum Electronics* **49**, 169 (2019).
 - [8] A. F. Molisch and B. P. Oehry, *Radiation trapping in atomic vapours* (Oxford University Press, Oxford, 1998).
 - [9] W. Happer, Y.-Y. Jau, and T. Walker, *Optically pumped atoms* (John Wiley & Sons, New York, 2010).
 - [10] M. Auzinsh, D. Budker, and S. M. Rochester, *Optically polarized atoms* (Oxford University Press, New York, 2010).
 - [11] W. Happer, *Rev. Mod. Phys.* **44**, 169 (1972).
 - [12] Y. Chang, Y.-H. Guo, and J. Qin, *Phys. Rev. A* **99**, 063411 (2019).
 - [13] W. Happer, E. Miron, S. Schaefer, D. Schreiber, W. A. van Wijngaarden, and X. Zeng, *Phys. Rev. A* **29**, 3092 (1984).
 - [14] T. G. Walker and W. Happer, *Reviews of Modern Physics* **69**, 629 (1997).
 - [15] T. Kornack and M. V. Romalis, *Physical review letters* **89**, 253002 (2002).
 - [16] Y.-Y. Jau, N. N. Kuzma, and W. Happer, *Physical review A* **66**, 052710 (2002).
 - [17] Z. Ma, E. Sorte, and B. Saam, *Physical review letters* **106**, 193005 (2011).
 - [18] D. Budker and M. Romalis, *Nat. Phys.* **3**, 227 (2007).
 - [19] V. V. Yashchuk, J. Granwehr, D. F. Kimball, S. M. Rochester, A. H. Trabesinger, J. T. Urban, D. Budker, and A. Pines, *Phys. Rev. Lett.* **93**, 160801 (2004).
 - [20] I. M. Savukov and M. V. Romalis, *Phys. Rev. Lett.* **94**, 123001 (2005).
 - [21] C. P. Slichter, *Principles of magnetic resonance*, Vol. 1 (Springer Science & Business Media, 2013).
 - [22] J. J. Sakurai and E. D. Commins, "Modern quantum mechanics, revised edition," (1995).
 - [23] B. C. Grover, E. Kanegsberg, J. G. Mark, and R. L. Meyer, "Nuclear magnetic resonance gyro," (1979), uS Patent 4,157,495.
 - [24] T. Kwon, J. Mark, and C. Volk, *Physical Review A* **24**, 1894 (1981).
 - [25] Z. Wu, W. Happer, and J. M. Daniels, *Phys. Rev. Lett.* **59**, 1480 (1987).
 - [26] Z. Wu, S. Schaefer, G. Cates, and W. Happer, *Physical Review A* **37**, 1161 (1988).
 - [27] P. Heimann, *Physical Review A* **23**, 1204 (1981).
 - [28] P. Heimann, I. Greenwood, and J. Simpson, *Physical Review A* **23**, 1209 (1981).
 - [29] E. A. Donley, J. Long, T. C. Liebisch, E. Hodby, T. Fisher, and J. Kitching, *Physical Review A* **79**, 013420 (2009).
 - [30] C. Gardiner and P. Zoller, *Quantum Noise: A Handbook of Markovian and Non-Markovian Quantum Stochastic Methods with Applications to Quantum Optics* (Springer, Berlin Heidelberg, 2004).
 - [31] D. F. Walls and G. J. Milburn, *Quantum Optics* (Springer, Berlin Heidelberg, 2008).

- [32] S. Appelt, A. B.-A. Baranga, C. J. Erickson, M. V. Romalis, A. R. Young, and W. Happer, *Phys. Rev. A* **58**, 1412 (1998).